

INVARIANT 3D SPHARM FEATURES FOR CHARACTERIZING FMRI ACTIVATIONS IN ROIS WHILE MINIMIZING EFFECTS OF INTERSUBJECT ANATOMICAL VARIABILITY

Ashish Uthama¹, Rafeef Abugharbieh¹, Samantha J. Palmer², Anthony Traboulsee² and Martin J. McKeown²

¹Biomedical Signal and Image Computing Laboratory, Department of Electrical and Computer Engineering, ²Department of Neurology, University of British Columbia, Vancouver V6T 1Z4, Canada

ABSTRACT

Spatial patterns of activation statistics within anatomically-defined regions of interest (ROIs) in functional magnetic resonance imaging (fMRI) data were recently shown to be sensitive markers of brain activation changes. Most current methods that analyze fMRI activation statistics largely ignore this. The accuracy and validity of the prevalent approach of spatial normalization of functional data is also being debated. In this paper we present a novel spherical harmonics based rotational, translation and scale invariant feature representation of fMRI data which allows for direct quantification of activation patterns within ROIs without any need for spatial normalization. We also present a novel parallel technique for quantifying anatomical properties of the ROIs where we employ a principal component based approach to reduce the effects of anatomical variability in the ROI on functional pattern analysis. We validate our proposed method and demonstrate its improved sensitivity over conventional methods using real and simulated fMRI data.

Index Terms— Spherical harmonics (SPHARM), invariant descriptors, functional magnetic resonance (fMRI), anatomical variability, spatial activation analysis.

1. INTRODUCTION

In recent years, functional magnetic resonance imaging (fMRI) has gained widespread recognition as an important means to study brain functionality. The functional response obtained over the duration of an fMRI experiment is analyzed on a voxel-by-voxel basis with the resultant activation statistics assembled into a statistical parameter map (SPM). The most common approach in generating an SPM is based on the general linear model (GLM) [1]. A key challenge in functional neuroimaging is in meaningfully combining results across subjects. The prevalent approach is to warp each subject's brain to a common atlas, thereby *normalizing* it. Current spatial normalization methods may give an imperfect registration result, resulting in signals from functionally distinct areas to be inappropriately combined [2]. Spatial normalization may therefore lead to poor sensitivity in the fMRI data analysis due to reduced functional overlap across subjects [3]. An alternate approach recently proposed [3] aligns subjects at the region of interest (ROI), as opposed to the whole brain level. These methods do not capture the spatial activation pattern of the data completely.

One of the first methods to study the spatial pattern of activation statistics used sums of activation statistics within

spheres of increasing radii [4]. However these features have limited sensitivity to spatial patterns since they only capture changes in the radial direction. A more sensitive approach by Ng *et al.* [5] employs three dimensional moment invariant features (3DMI). However, both these methods do not account for intersubject variability present in the ROI masks and its effect on the analysis.

In [8], the use of invariant SPHARM descriptors for analyzing convex anatomical structures (represented as binary 3D shapes) in magnetic resonance was proposed. SPHARM-based methods have previously been proposed in the context of 3D shape retrieval systems [6, 7] which are not limited to convex topologies. These methods proposed obtaining invariant SPHARM features by intersecting 3D shapes with shells of growing radii. This approach, however, could not detect independent rotations of a shape along the shells, thereby resulting in a non-unique representation [7]. In order to overcome this limitation, we have recently proposed a unique radial transform [9].

In this paper, we extend our SPHARM-based representation to characterize the full 3D spatial fMRI activation pattern within an ROI. Each ROI feature is invariant to similarity transformations, so mutual alignment of subject brains (or ROIs) is not needed. The other contribution of our proposed approach is in the novel way we account for the underlying structural (anatomical) inter-subject variability in the ROI binary masks using a subspace projection method. We validate our proposed technique on realistic simulated fMRI data and demonstrate improved sensitivity compared to the ROI-based normalization method [3]. Furthermore, we demonstrate the practical significance of our work using real data from an fMRI experiment conducted on subjects with Parkinson's disease (PD).

2. METHODS

2.1. Invariant SPHARM-based spatial features

A 3D object can be represented in the spherical coordinate system as $\Psi(r, \theta, \phi)$, where r is the distance from the origin, θ is the zenithal angle and ϕ is the azimuthal angle. Burel and Henocq proposed using the spherical harmonic expansion of such a function (1) to obtain rotationally invariant features [10]. $Y_{lm}^*(\theta, \phi)$ in (1) are the complex conjugate of the m^{th} order spherical harmonic basis functions of degree l . l ranges from 0 to L , the bandwidth (explained later). k is the radial index.

$$c_{kl}^m = \int_0^\infty r^2 dr \int_0^{2\pi} d\phi \int_0^\pi \sqrt{2} \frac{\sin(\pi kr)}{r} Y_{lm}^*(\theta, \phi) \Psi(r, \theta, \phi) \sin(\theta) d\theta \quad (1)$$

Direct computation of (1) to characterize 3D functions is highly inefficient [11] and has thus not been used in a practical application. In [9] we proposed an alternate approach to compute this representation using concentric spherical shells and a radial transform. This representation enabled us to use a more computationally efficient transform described by Healey *et al* [11]. The origin of the shells is placed at the centre of mass of the 3D function's equivalent binary mask to nullify translational effects. By representing the data as a set of spherical functions obtained by intersecting the 3D data with concentric shells of unit voxel thickness, we were able to simplify (1) into (2) and (3) (where r and k enumerate the shell numbers).

$$c_{kl}^m = \sum_{r=1}^{2R_{\max}} r^2 \sqrt{2} \frac{\sin(\pi r)}{r} c_{rl}^m \quad k = [1, 2, 3, \dots, S_{\max}] \quad (2)$$

$$c_{rl}^m = \int_0^{2\pi} d\phi \int_0^\pi Y_{lm}^*(\theta, \phi) \Psi(r, \theta, \phi) \sin(\theta) d\theta \quad r = [1, 2, 3, \dots, S_{\max}] \quad (3)$$

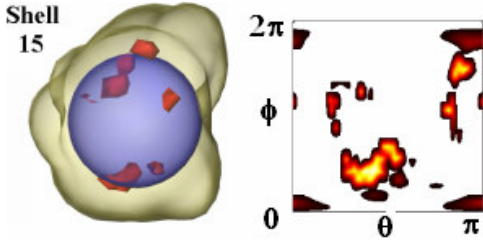


Figure 1. Real fMRI data from the right cerebellar hemisphere is shown on the left (only activation values above $t=2$ shown for clarity). The intersection of the data with a shell is shown on the right. The physical values of both spherical angles are non-uniformly spaced (Chebyshev nodes) [11].

S_{\max} is the number of spherical shells used. To enable a scale invariant representation across a set of 3D functions, a common number of shells, S_{\max} , has to be evenly spaced within the extent of each function separately. For a cubic voxel grid, the spacing between the shells has to be at maximum, 0.5 voxels wide to enable fair sampling of all voxels. We first find the 3D function with the largest radius from the origin to the outer most non-zero point (measured in terms of voxels) R_{\max} . To ensure that the spacing constraint is met for all functions, S_{\max} is then set to be $2R_{\max}$.

Surface sampling along each of these shells is performed on an equiangular spherical grid of dimensions $2L \times 2L$ [11], where L is the bandwidth. This common bandwidth L for all shells of all functions is chosen to satisfy the sampling criterion for the largest shell, the one with radius R_{\max} . Recognizing that in applications pertaining to discrimination, high accuracy in the SPHARM representation is not a necessity, we use a heuristic approach based on the surface area to determine an adequate bandwidth. The surface area for the largest shell represents the maximum surface shell area (in terms of voxels) that the sampling grid needs to span; hence the minimum value for L is obtained by equating the surface area of this largest shell to the equiangular sampling grid (4).

$$4\pi R_{\max}^2 = 2L \times 2L, L = R_{\max} \sqrt{\pi} \quad (4)$$

From the SPHARM representation (2) so obtained, we compute rotationally invariant features using (5) as outlined in [10]. h and i are used to index these features. Note that we reshape I into a single row vector, termed the feature vector, of dimensions $D = L \times 2R_{\max}$ for later analysis.

$$I(h, i) = \sum_{k=1}^{2R_{\max}} \sum_{m=-l}^{m=l} c_{kl}^m (c_{kl}^m)^*, h = 1 \dots L, i = 1 \dots 2R_{\max} \quad (5)$$

2.2. Obtaining functional SPHARM features

In an ROI based fMRI analysis experiment, the collected data can be viewed as having two parts. The *binary* ROI mask resampled from the high resolution anatomical scan contains only the structural information, whereas, the fMRI ROI statistics obtained by masking the whole brain SPM with this binary ROI mask contains *both* structural and functional data. The proposed method first derives SPHARM feature vectors as defined in section 2 (5) for both these functions (binary ROI mask and fMRI ROI statistics) using an R_{\max} value obtained considering all subjects. This ensures that all feature vectors obtained are of the same size D and are in the same scale, translation and rotationally invariant feature space. The SPHARM features obtained from the binary ROI mask are termed *SPHARM-s* (*structural*) since they capture only the structural aspects of the ROIs. The features obtain from the fMRI ROI statistics are termed *SPHARM-fs* (*function + structure*). These features are influenced by two factors. The first factor, which is the one of interest, is the functional aspect exhibited by the spatial pattern of the activation statistics within the ROI. The second factor is the shape of the anatomically-defined ROIs. In functional studies this *structural* information reflects inter-subject variability, which adversely affects the primary aim of the analysis: resolving *functional* pattern changes across subject groups.

To ensure no systematic bias enters the analysis during group discrimination (*e.g.* when trying to discriminate functional response of control subjects from PD patients), we first pool all the structural feature vectors (*SPHARM-s*) from both groups into a single matrix. Orthogonal projections of this matrix are then obtained using principal component analysis (PCA). The first d (usually observed to be 3) directions obtained reflect up to 97% of the unwanted effects of intersubject variability in structure of the ROIs. By projecting the pooled *SPHARM-fs* on the remaining $D-d$ directions (directions which are minimally effected by structural variations), we obtain a new set of features which we term *SPHARM-f*. These features are minimally affected by structural variations, and thus ensure that subtle functional pattern changes will not be obscured by structural inter-subject variability. We further validate this claim with synthetic data experiments.

2.3. Statistical group analysis

To efficiently discriminate two groups of 3D fMRI distributions, we first derive *SPHARM-f* features for each subject's ROI as explained in section 2. To determine the level of statistical significance in the difference between the groups, we employ a non-parametric permutation test as explained by Vesta *et al* [12]. Permutation tests generate the null distribution of a hypothesis from the data itself and hence do not need a prior assumption of its parameters. This makes it well suited for the analysis of long feature vectors whose generating probability distributions are not easily definable. This test results in a p value. If this value is below the statistical standard threshold of $\alpha = 0.05$ is considered as an indication that significant difference exists between the groups being analyzed.

2.4. ROI normalization approach (ROI-N)

To demonstrate practical advantages of the discriminatory powers of the proposed approach, we compare results with those obtained from spatial normalization of the ROIs. We use an improved version of the ROI-AL method proposed by Stark and Okada [3].

A non-linear spatial normalization approach [13] is used to obtain the parameters required to warp each subject's anatomical T1 ROI to the template instead of the rigid registration proposed in [3]. A final test for difference in means across groups is performed at each voxel location yielding a group level t-statistic map. A *height* threshold is then applied to retain voxels that have significantly different means between the two groups. We then apply a *cluster size* threshold [14]. Existence of at least one surviving cluster after these thresholdings is taken as an indication that the groups being analyzed have a significant difference between them.

3. DATA

3.1. Simulated fMRI data

Synthetic fMRI data sets were generated using binary ROI masks obtained from real MR data. Ten binary ROI masks of the right cerebellar hemisphere were obtained from the control subject group of our fMRI study. R_{max} was found to be 19 voxels, corresponding to 57mm at 3mm voxel resolution. Spatial activation noise is generated from normally distributed values with zero mean and unit variance. To mimic the intrinsic spatial correlation of fMRI data, the values are spatially smoothed using a Gaussian kernel (FWHM = 3.5mm). To obtain a functional centroid for the synthetic pattern, the centroid of each binary mask is randomly jittered by up to three voxels in all three spatial directions. This corresponds to a maximum displacement of 12.7mm at a resolution of 3mm×3mm×3mm per voxel. An activation pattern, modeled after the examples used by Kontos and Megalookonomou [4], is then generated by setting all voxels within a distance of 5 voxels from the chosen centroid to a value δ . While voxels at a distance between 5 to 10 voxels are set to $-\delta$. The magnitude of δ can be varied to obtain the desired SNR. This pattern is smoothed using a Gaussian kernel (FWHM = 3.5mm) before adding the independently generated noise explained earlier.

3.2. Real fMRI data

This study was approved by the University of British Columbia Ethics Board. 10 volunteers with clinically diagnosed PD participated in the study. 10 healthy, age-matched control subjects were also recruited. Subjects performed a bulb squeezing task at two different rates interspersed with steady periods. Each task (block) lasted for 20 seconds repeated for a total of 4 minutes. A Philips Achieva 3.0 T scanner equipped with a head-coil was used. Echo-planar T2*-weighted images with blood oxygenation level-dependent (BOLD) contrast were acquired. Scanning parameters were: repetition time 2000 ms, echo time 3.7, flip angle 90°, field of view 240.00 mm, matrix size = 128 x 128, pixel size 1.9 x 1.9 mm. Each functional run lasted 260 seconds. 36 axial slices of 3mm thickness were collected in each volume, with a gap thickness of 1mm. A high resolution, 3-dimensional T1-weighted image consisting of 170 axial slices was acquired of the whole brain.

The functional MRI data were pre-processed using trilinear interpolation for 3D motion correction and Sinc interpolation for slice time correction. The data were then motion corrected and manually segmented to obtain ROIs based on anatomical landmarks. Sixteen ROI's, hypothesised to be involved in motor tasks, were drawn separately in each hemisphere. They were outlined on the unwarped, aligned structural scan for each subject using Amira software. The ROIs are: primary motor cortex (M1), supplementary motor cortex (SMA), prefrontal cortex (PFC), caudate (CAU), putamen (PUT), thalamus (THA), cerebellum (CER) and anterior cingulate cortex (ACC). The labels on the

segmented anatomical scans were resliced at the fMRI resolution. A hybrid Independent Component Analysis (ICA) / General Linear Model scheme [15] was used to contrast and create statistical parametric maps (SPMs).

4. RESULTS AND DISCUSSION

4.1. Validation on Synthetic Data

Two synthetic data sets were generated, one with no signal (only noise) and another with a known non-zero signal value. Signal to noise ratio (SNR) was controlled by the magnitude of δ . By incrementing the SNR value in steps and using the SPHARM and ROI-N approach to discriminate the noise-only and signal+noise group at each SNR value, relative sensitivities of the methods were observed. Figure 2 summarizes the performance of the SPHARM approach. *SPHARM-fs* features are able to discern a difference in the two groups at -3.4 dB and higher. *SPHARM-f* features perform better, picking up the difference at an SNR value of -10.7 dB.

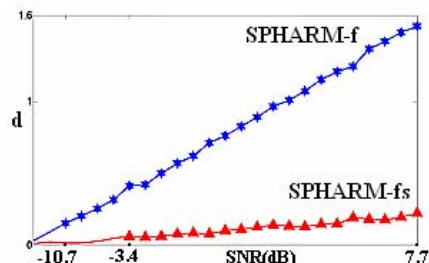


Figure 2. Sensitivity of the SPHARM approach. The mean Euclidean distance (d) between the feature vectors of a group with only noise and of another group with increasing SNR is plotted against the SNR. The star and triangle markers denote distance which yielded a p value less 0.05, signifying that the method detected differences between the groups.

Figure 3 presents the results of the ROI normalization approach for different height thresholds. Hayasaka *et al* [14] have shown that results are sensitive to the height threshold and cluster size threshold used, both of which are dependent on the estimated *smoothness* of the data. Based on their simulation results, we use a very liberal cluster size threshold of 4 connected voxels (26 voxel neighborhood) corresponding to zero smoothness. Height thresholds of 2, 3 and 4 were used. A value of 2 corresponds to an *uncorrected* (for multiple comparisons) p value of 0.0304 with 18 degrees of freedom. This experiment shows that the sensitivity of

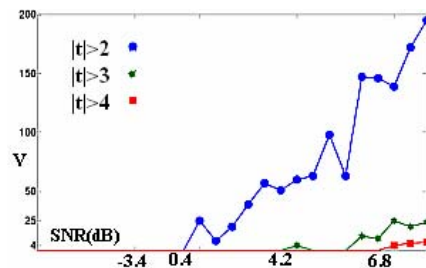


Figure 3. Sensitivity of the ROI-normalization approach. The number of voxels (V) surviving various height thresholds (2, 3 and 4) is plotted against the SNR. A cluster size threshold of 4 connected voxels was used in each case.

both the SPHARM approaches outperforms the ROI-N method. *SPHARM-f* features perform better than *SPHARM-fs* features indicating the advantage of the principal component subspace approach in reducing intersubject structural variations. The graphs

for both SPHARM methods show a consistent trend emphasizing the robustness of the method to noise. The ROI-N method shows a higher susceptibility to noise, especially the $t > |3|$ graph in Figure 3.

4.2 Application to Clinical fMRI Data

SPHARM-*fs* and SPHARM-*f* features were derived for all participants as outlined in section 2. Table I displays the result of the SPHARM analysis. The table only shows ROIs for which at least one test found a significant difference in the activation patterns between the two frequencies ($\alpha=0.05$).

ROI	SPHARM- fs Normals	SPHARM- f Normals	SPHARM- fs PD	SPHARM- f PD
L_CER	0.0613	0.4694	0.0239*	0.0202*†
L_M1	0.1767	0.1761	0.0863	0.0104*
L_PFC	0.5302	0.9497	0.1045	0.0378*
L_THA	0.1200	0.0425*	0.0651	0.2513
R_CER	0.0546	0.1599	0.0478*	0.0309*†
R_PFC	0.6938	0.5273	0.0150*	0.0166*

Table 1. SPHARM analysis of the two frequency tasks, N=10,000 permutations were performed. † ROIs detected by ROI-N.

The Sixteen ROIs from the twenty subjects were also analyzed using ROI-N. We used a range of height thresholds varying from 2 to 5 in steps of 0.5, while using a cluster size threshold of 4. Among the 32 combinations of tests performed (2 subject groups with 16 ROIs), only the left and the right cerebellar hemispheres in the PD group had at least one cluster left.

These results demonstrate that using the standard ROI normalization approach, increased movement rate was associated with an increase in activity of the cerebellum bilaterally in PD subjects, but not in healthy controls. This is consistent with an increased reliance on visual feedback in PD subjects mediated by the cerebellum [16]. The SPHARM-*fs* features, in addition, were able to detect changes in the activation of the ipsilateral prefrontal cortex of PD subjects. This region is associated with performance monitoring, thus a change in the activity of this area may reflect an increased attentional demand in PD subjects as the movement becomes more difficult. The SPHARM-*f* approach, in which structural variations in ROI anatomy across subjects are minimized, showed greater sensitivity. Specifically, control subjects showed a change in the activation of contralateral thalamus with increasing movement rate, consistent with an increased output from the basal ganglia. PD subjects were apparently not able to adjust the output through the thalamus, and instead showed adjustments in the output from bilateral cerebellum, bilateral prefrontal cortex, and contralateral M1 in response to increased task demands. Increased activity of M1 and cerebellum in PD has previously been suggested to be a compensatory mechanism [17]. It is thus possible that compensatory mechanisms are recruited during tasks which make greater demands on the motor system, and rely on changes to the shape as well as the level of activation.

5. CONCLUSIONS

In this paper, we proposed a new technique for analyzing spatial activation patterns in fMRI data using 3D SPHARM features. The features, which are unique to an ROI, were obtained by intersecting 3D data distributions with concentric shells of increasing radii followed by a radial transform. Our other main contribution was a novel approach to account for anatomical shape variations across subjects while discriminating subtle changes in

spatial distribution of fMRI activation patterns within an ROI. The effectiveness of the proposed approach in mitigating structural variability, robustness to noise and comparative sensitivity were validated on synthetic data. We also demonstrated our method's ability to discriminate functional pattern changes within anatomical ROIs in real fMRI data. By applying our spatial analysis technique, we were able to demonstrate differences in the way that PD subjects and healthy controls respond to an increased task demand, reflecting failure of PD subjects to increase basal ganglia output, and a reliance on cerebellar and cortical activity to enable successful performance. This adjustment may reflect a compensatory mechanism in PD subjects. An interesting application of the proposed approach would be to compare activation patterns between subject groups that are expected to have systematic changes in both structural and functional aspects.

REFERENCES

- [1] K. J. Friston, A. P. Holmes, K. J. Worsley, J. B. Poline, C. Frith and R. S. J. Frackowiak, "Statistical Parametric Maps in Functional Imaging: A General Linear Approach," *Human Brain Mapping*, pp. 189-210, 1995.
- [2] M. Ozcan, U. Baumgartner, G. Vucurevic, P. Stoeter and R. Treede, "Spatial resolution of fMRI in the human parasyllvian cortex: Comparison of somatosensory and auditory activation," *Neuroimag*, pp. 877, 2005.
- [3] C. E. Stark and Y. Okado, "Making memories without trying: medial temporal lobe activity associated with incidental memory formation during recognition," *Journal of Neuroscience*, pp. 6748-6753, 2003.
- [4] D. Kontos and V. Megalooikonomou, "Fast and effective characterization for classification and similarity searches of 2D and 3D spatial region data," *Pattern Recognition*, vol. 38, pp. 1831-1846, 2005.
- [5] B. Ng, R. Abugharbieh, X. Huang and M. J. McKeown, "Characterizing fMRI activations within regions of interest (ROIs) using 3D moment invariants," in *MMBIA*, 2006.
- [6] D. V. Vranic, "An improvement of rotation invariant 3D-shape based on functions on concentric spheres," pp. 757-60, vol.2, 2003.
- [7] M. Kazhdan, T. Funkhouser and S. Rusinkiewicz, "Rotation invariant spherical harmonic representation of 3D shape descriptors," in *Symposium on Geometry Processing*, pp. 156-65, 2003.
- [8] S. Tootoonian, R. Abugharbieh, X. Huang and M. J. McKeown, "Shape vs. volume: Invariant shape descriptors for 3D region of interest characterization in MRI," in *ISBI*, pp. 754-757, 2003.
- [9] A. Uthama, R. Abhugharbieh, A. Traboulsee and M. J. McKeown, "Invariant SPHARM shape descriptors for complex geometry MR region of interest analysis in MR region of interest analysis," *EMBC*, pp.1322, 2007.
- [10] G. Burel and H. Henocq, "Three-dimensional invariants and their application to object recognition," *Signal Processing*, pp. 1-22, 1995.
- [11] D. M. Healy, D. N. Rockmore, P. J. Kostelec and S. Moore, "FFTs for the 2-Sphere-Improvements and Variations," *Journal of Fourier Analysis and Applications*, vol. 9, pp. 341-385, 2003.
- [12] Y. S. K. Vetsa, M. Styner, S. M. Pizer, J. A. Lieberman and G. E. Gerig, *Caudate Shape Discrimination in Schizophrenia using Template-Free Non-Parametric Tests*, pp. 661-669, 2003.
- [13] J. Ashburner and K. J. Friston, "Nonlinear spatial normalization using basis functions," *Human Brain Mapping*, vol. 7, pp. 254-266, 1999.
- [14] S. Hayasaka and T. E. Nichols, "Validating cluster size inference: random field and permutation methods," *Neuroimage*, pp.2343-2356, 2003.
- [15] M. J. McKeown, L. K. Hansen and T. J. Sejnowski, "Independent component analysis of functional MRI: what is signal and what is noise," *Current Opinion in Neurobiology*, vol. 13, pp. 620-629, 2003.
- [16] J. F. Stein and M. Glickstein, "Role of the cerebellum in visual guidance of movement," *Physiol. Rev.*, vol. 72, pp. 967-1017, Oct. 1992.
- [17] S. Thobois, P. Dominey, J. Decety, P. Pollak, M. C. Gregoire and E. Broussolle, "Overactivation of primary motor cortex is asymmetrical in hemiparkinsonian patients," *Neuroreport*, vol. 11, pp. 785-789, 2000.